 doi:10.20944/preprints202111.0234.v1

Article

On the Arrangement of Pentagonal Columns in Tetragonal Tungsten Bronze-Type $Nb_{18}W_{16}O_{93}$

Frank Krumeich[1]*

[1] Laboratory of Inorganic Chemistry, Department of Chemistry and Applied Biosciences, ETH Zürich, 8093 Zürich, Switzerland
* Correspondence: krumeich@inorg.chem.ethz.ch

Abstract: The evaluation of HAADF-STEM images of a sample with the composition $Nb_{18}W_{16}O_{93}$ provided new insights in its real structure. The basic structure comprises an intact octahedral framework of the tetragonal tungsten bronze (TTB) type. The partial occupation of the pentagonal tunnels (PT) by metal-oxygen strings determines the oxygen to metal ratio (O/ΣM with M = Nb,W). For a large area, the O/ΣM was determined to be 2.755 which is smaller than the value of $Nb_{18}W_{16}O_{93}$ which is O/ΣM = 2. 735. To a large extent, the threefold TTB superstructure structure of $Nb_8W_9O_{47}$ with a high oxygen content is present (O/ΣM = 2.765). In addition, a new fourfold TTB superstructure was found in small domains: $Nb_{12}W_{11}O_{63}$ with an O/ΣM = 2.739 obviously accommodates a part of the sample's metal excess compared to the stable phase $Nb_8W_9O_{47}$.

Keywords: niobium tungsten oxide; pentagonal tunnels; tetragonal tungsten bronze; high-angle annular dark field detector; scanning transmission electron microscopy; HAADF-STEM; twinning; superstructure, battery material.

1. Introduction

At present, there is a broad interest in niobium tungsten oxides since they have application potential as high-performance anode materials in lithium ion batteries. The recent world-wide research activities have been induced in 2018 by a report of extremely fast reversible Li exchange and high cycling stability for the block-type phase $Nb_{16}W_5O_{55}$ and for a sample with the composition $Nb_{18}W_{16}O_{93}$, the structure of which was found to be based on the tetragonal tungsten bronze (TTB) type [1]. This structure type comprises corner-sharing octahedra MO_6 that are arranged in such a way that trigonal, square, and pentagonal tunnels arise (Figure 1, bottom left). In the structure of $Nb_8W_9O_{47}$, one third of the pentagonal tunnels (PTs) are systematically occupied by metal-oxygen (MO) strings resulting in a threefold superstructure of the TTB type (Figure 1, top). The metal inside the PT has got a pentagonal bi-pyramidal coordination by oxygen. The unit comprising this polyhedron and the five equatorially connected octahedra is designated a pentagonal column (PC) [2]. Two of such PCs are grouped to pairs by sharing a square of octahedra (so-called diamond link [2]). Four orientations of these PC pairs are possible in the TTB framework, and at a time two of them occur in each of the two unit cell orientations of the $Nb_8W_9O_{47}$ structure (Figure 1). The threefold TTB superstructure realized in $Nb_8W_9O_{47}$ exhibits a high thermodynamic stability, apparently because the interactions between the MO strings inside the TTB substructure are optimized in this arrangement. Iijima and Allpress postulated rules for a stable dense packing of PCs [3]: (i) PTs directly adjacent to a PC ($d_{PC\text{-}PT} \approx 0.6$ - 0.65 nm) remain empty; (ii) one of the two PTs with the next-nearest distance to a PC ($d_{PC\text{-}PT} \approx 0.9$ nm) is occupied forming a pair of diamond-linked PCs. These rules are strictly obeyed in the structure of $Nb_8W_9O_{47}$. Any deviation from the composition $M_{17}O_{47}$ (M = Nb,W) therefore leads to a less ordered real structure. An occupation of

Preprints (www.preprints.org) | NOT PEER-REVIEWED | Posted: 12 November 2021 doi:10.20944/preprints202111.0234.v1

directly adjacent PTs, which breaches the first rule, has rarely been observed in TTB-type niobium tungsten oxides up to now. In contrast, the second rule is strictly valid for the composition $M_{17}O_{47}$ only and chains of diamond-linked PCs have frequently been observed in W-richer structural variants like $Nb_6W_8O_{39}$ (Figure 1) [4].

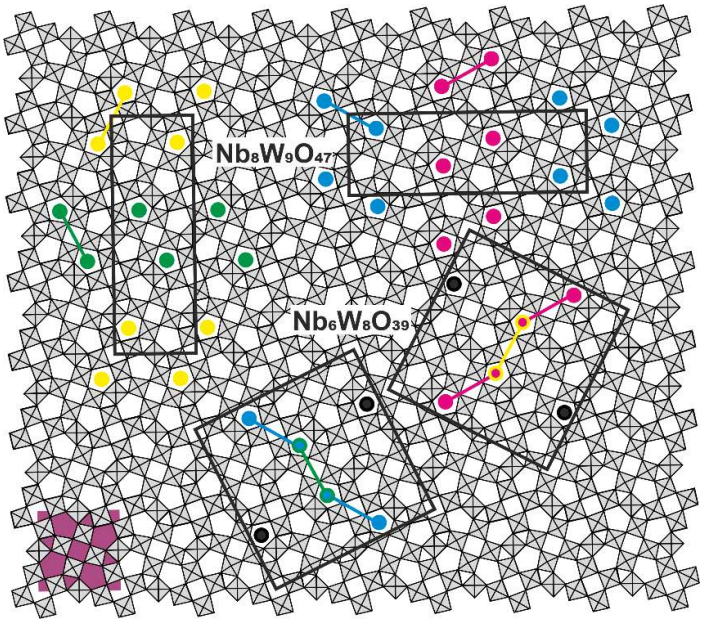

Figure 1. Structural models of $Nb_8W_9O_{47}$ and of $Nb_6W_8O_{39}$ in projection along [001]. Two possible orientations of both structures are shown (unit cells are framed). Filled pentagonal tunnels (PTs) are represented by filled circles. Pairs of filled PTs (filled circles of same color) are connected via the diamond link (some marked by colored lines). A TTB subcell with composition $M_{10}O_{30}$ (M = Nb,W) is colored purple.

Already in 1979, Li-containing phases $Li_xNb_8W_9O_{47}$ with x = 2 and 4 could be synthesized by the reaction of $LiNbO_3$ and WO_3 [5]. In 1998, the insertion of Li into $Nb_8W_9O_{47}$ by both electrochemical and chemical reactions could be achieved [6]. A reversible electrochemical uptake of up to 20 Li ions per formula unit was reported for $Nb_8W_9O_{47}$ and for the not fully oxidized members of the solid solution series $Nb_{8-x}W_{9+x}O_{47}$ ($1 \leq x \leq 6$) [7]. As already mentioned above, the electrochemical investigations on TTB-type NbW oxides gained momentum after the study on $Nb_{18}W_{16}O_{93}$ had been published by Griffith et al. in 2018 [1]. Several follow-up investigations confirmed the outstanding electrochemical performance of samples with this composition [8-13]. An orthorhombic structure $Nb_{18}W_{16}O_{93}$ was proposed by Stephenson in 1968 to explain split reflections observed in higher order Laue zones of a twinned crystal with the composition $Nb_{12}W_{11}O_{63}$ ($6Nb_2O_5$:$11WO_3$) [14]. For this composition, congruent melting was found in the course of the exploration of the phase diagram Nb_2O_5/WO_3 by Roth and Waring [15]. The structure of the hypothetical $Nb_{18}W_{16}O_{93}$ could never been confirmed, neither by single crystal X-ray diffraction nor by transmission electron microscopy studies [3,16,17]. As both the structural model of $Nb_{18}W_{16}O_{93}$ and the well-established phase $Nb_8W_9O_{47}$ are described by a threefold TTB superstructure with similar symmetry and practically the same unit cell metric, the differentiation of the two structures by powder XRD is difficult but possible if a comparative Rietveld refinement is performed [18]. The difference between these structures is the occupation of PTs in the TTB host lattice, and thus the appropriate characterization method is to image the metal positions in the **ab** plane by high-resolution transmission electron microscopy (HRTEM) [3,19] or by high-angle annular dark field scanning transmission electron microscopy (HAADF-STEM) [20-22]. The conclusions drawn from the analysis of HAADF-STEM images of a sample $Nb_{18}W_{16}O_{93}$ are reported here.

2. Materials and Methods

2.1. Synthesis

The sample with composition $Nb_{18}W_{16}O_{93}$ was prepared by the solid state reaction of Nb_2O_5 and WO_3 powers (molar ratio Nb_2O_5:WO_3 = 9:16). After grinding the powders in an agate mortar, the resulting mixture was pressed into pellets and then annealed in a Pt crucible covered with a Pt lid at 700 °C for 12 h followed by 1200 °C for 12 h. For details, see [12].

2.2. Electron Microscopy

Scanning transmission electron microscopy images were recorded on a JEM-ARM300F (JEOL) using a high-angle annular dark field detector (HAADF-STEM), as described elsewhere [12].

3. Results

HAADF-STEM images of all crystal fragments observed here along the short crystallographic **c** axis reveal a defect-free TTB substructure (Figures 2a, 3a, 5a). A close examination of the images shows that most PTs are empty as recognizable by five bright dots corresponding to a pentagon of octahedra MO_6 centered by a black patch. Filled PTs (PCs) are likewise imaged as a pentagon of bright dots centered by a sixth one (Figure 2a). The arrangement of the PCs in large areas corresponds to that of $Nb_8W_9O_{47}$ (Figure 1), e. g. in the upper half of Figures 2a. In the lower part of Figures 2a, a domain with a hitherto unobserved structure occurs: like in the $Nb_8W_9O_{47}$ structure, two differently oriented PC pairs are present (marked yellow and blue in Figures 2b,c). In this structure, they are oriented nearly perpendicular in respect to each other so that two regularly arranged PCs are directly adjacent to each other (red arrows in Figure 2d). While this close distance breaks the first rule proposed for a stable PC arrangement, it enables a denser PC packing and thus a decrease of the oxygen/metal ratio O/ΣM (M = Nb,W). A fourfold TTB supercell with $a = b = a_{TTB}$, $c = c_{TTB}$ describes this structure (Figures 2d). The metric of this cell is approximately tetragonal, but the peculiar PC arrangement decreases its symmetry to orthorhombic. In this cell, six of the sixteen PTs are occupied according to $(MO)_6(M_{10}O_{30})_4$ or normalized to a single TTB unit $(MO)_{1.5}(M_{10}O_{30})$. Thus, the number of PCs is higher than in $Nb_8W_9O_{47}$ corresponding to $(MO)_{1.33}(M_{10}O_{30})$, which moreover leads to a decreased ratio O/ΣM: 2.739 vs. 2.765. The general formula $(MO)_6(M_{10}O_{30})_4$ corresponds to a composition $Nb_{12}W_{11}O_{63}$, which is that of the so-called 6:11 phase ($6Nb_2O_5$:$11WO_3$) [15]. Interestingly, the structural model contains TTB cells in which all four PTs are empty as indicated by red frames in Figure 2d, an array that does not occur in the $Nb_8W_9O_{47}$ structure. These empty TTB units and such in which two PTs are occupied (blue PC pairs) are alternatingly arranged in the structural model of $Nb_{12}W_{11}O_{63}$ (Figure 2d). The domains of $Nb_8W_9O_{47}$ and $Nb_{12}W_{11}O_{63}$ are intimately intergrown with each other by sharing a slab of PC pairs (yellow in Figure 2c) that run along the crystallographic **a** axis of $Nb_8W_9O_{47}$. The domain of the new structure is terminated on the left side by a defective area which contains the blue PC pairs as a slab in perpendicular orientation.

A larger area which contains mainly the $Nb_8W_9O_{47}$ structure is shown in Figure 3. Two distinct defects that are typical for this structure occur, namely an out-of-phase boundary on the lower left side and rotational twinning by 90° on the right side. The threefold TTB superstructure is perfectly ordered on the upper left side (Figure 3a). The inclusion of a row of five PC pairs with perpendicular orientation (blue) causes a shift of the adjacent domains of $Nb_8W_9O_{47}$ by 1/3 **b** (= $\mathbf{b}_{TTB}$) in respect to each other (Figure 3b,c). In the lower part of the boundary, the structure is semiregular: the slabs of yellow PC pairs in the two domains are connected via a chain of four diamond-linked PCs with each slab contributing two PCs. The slabs with green PC pairs are not connected. Instead, they are directly neighbored to an isolated yellow PC.

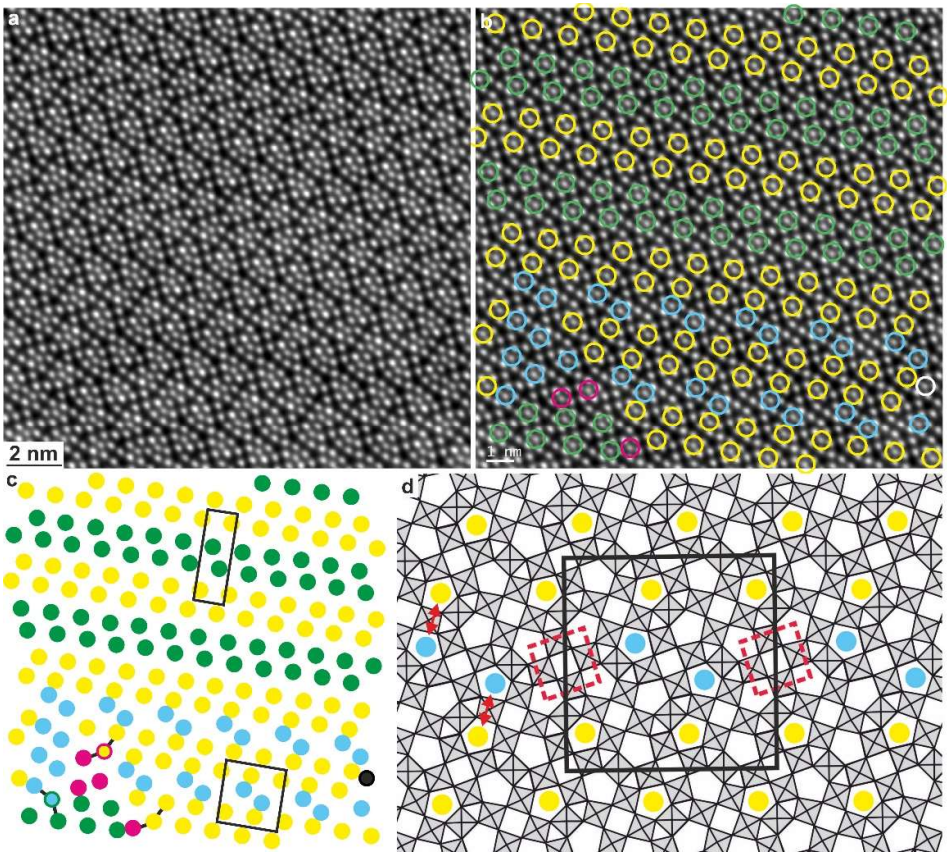

Figure 2. (a) HAADF-STEM image of $Nb_{18}W_{16}O_{93}$ recorded along [001] (courtesy of Prof. L. Shen, Nanjing) and (b) with the filled PTs marked as open circles. Pairs of diamond-linked pentagonal columns (PC) with the same orientation have the same color. (c) Scheme of the PCs with unit cells of $Nb_8W_9O_{47}$ (top) and $Nb_{12}W_{11}O_{63}$ (bottom) outlined. (d) Structural model of $Nb_{12}W_{11}O_{63}$. Red double arrows mark two directly adjacent PCs, dashed squares empty TTB units. For details, see text. Figure 2a has been published in modified form as Figure 2e in [12] under CC-BY license.

This structure is depicted in the lower left side of Figure 4a. Four-membered PC chains had been observed before, e. g. in zigzag out-of-phase and twin boundaries in $Nb_8W_9O_{47}$ [3] and as a regular structural element in $Nb_6W_8O_{39}$ (Figure 1) [4]. At the top of this boundary, the occupation of PTs is less regular and includes a three-membered PC chain, in which die middle PC belongs to two perpendicularly oriented slabs of PC pairs (blue and green). Here, a small block of six PCs with perpendicular orientation (90° rotation twin) is incorporated (light blue area). Interestingly, this block connects two slabs of green PC pairs, and the two PCs at the top and at the bottom can be regarded as a part of the small section of 3 PC pairs (light blue area) as well as a part of the connected slabs of green PCs.

Another example for such rotational twinning appears on the right side of Figure 3 with the corresponding structural model shown in Figure 4b. In the upper part, slabs of blue and magenta PC pairs are connected to perpendicularly oriented slabs of green and yellow PC pairs. The arrangement there is frequently observed at boundaries between rotational twin domains: the central PC of a triple PC chain belongs to the two perpendicular PCs slabs. This is also the case of the isolated PC that is quasi the extension of the not directly connected PC rows. This frequently appearing array is marked by dotted lines for the two just described units in Figure 4b (top center). It should be mentioned that such a connection of 90° rotational twin domains by three-membered PC chains was already observed in the first HRTEM investigation of this material in 1974 [3]. Like here, empty TTB cell and directly adjacent simultaneously occupied PTs were found then.

 doi:10.20944/preprints202111.0234.v1

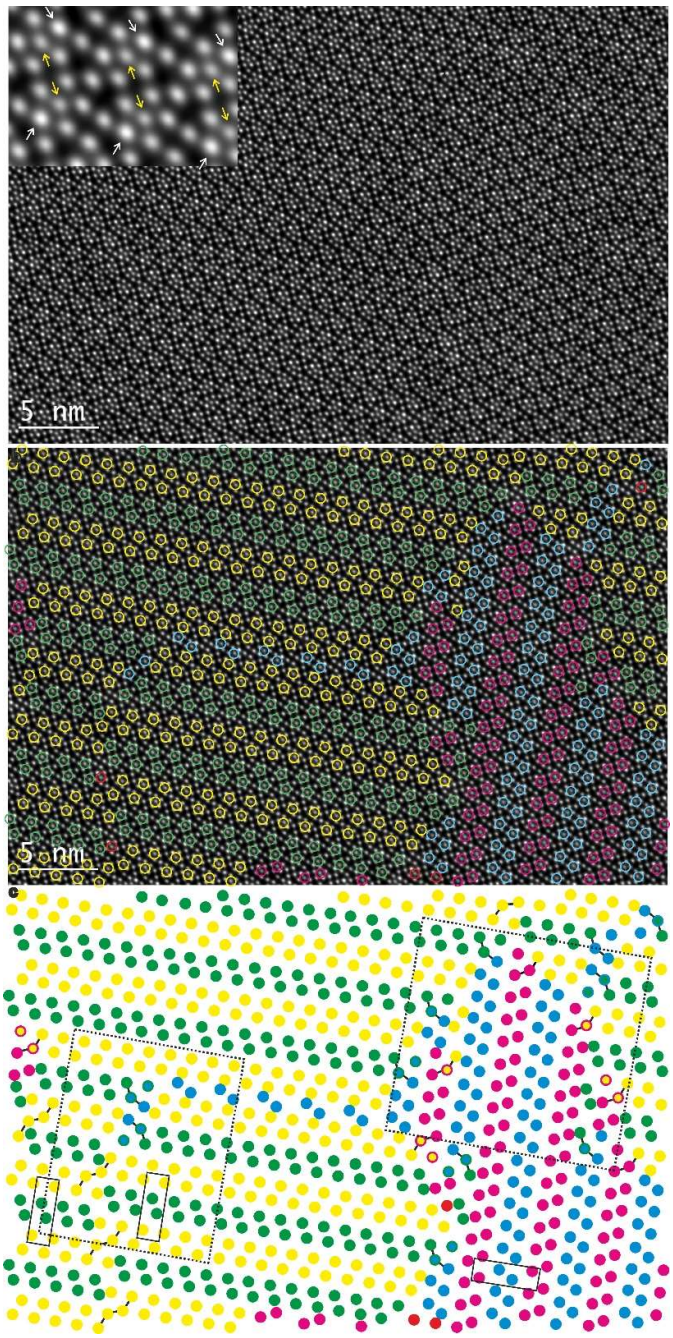

Figure 3. (a) HAADF-STEM image of $Nb_{18}W_{16}O_{93}$ recorded along [001] (courtesy of Prof. L. Shen, Nanjing) and (b) with the filled pentagonal tunnels (PTs) marked as open circles. (c) Scheme of the PT array. Rectangles framed by solid lines indicate unit cells of $Nb_8W_9O_{47}$ and by dotted lines the areas interpreted in Figure 4. The magnified area (inset in (a)) demonstrates the varying dot intensities with white arrows pointing to W-rich and yellow ones to Nb-rich positions, respectively.

As the HAADF-STEM method generates images with the intensity I increasing with the atomic number Z ($I \sim Z^2$; Z contrast imaging [23]), the metal positions appear as bright dots with their brightness increasing with the W content of the particular atomic column ($Z_W = 74 > Z_{Nb} = 41$)[19,21]. Thus, the observation of the relative brightness of the individual atomic columns provides some information about the distribution of the metals (inset in Figure 3a). The relative darkness of the metal position inside the PTs indicates that is preferentially occupied by Nb as it is also the case in W-richer samples [21]. Thus, the

Preprints (www.preprints.org) | NOT PEER-REVIEWED | Posted: 12 November 2021 doi:10.20944/preprints202111.0234.v1

preference of Nb for this position as it was found during the structure determination of $Nb_8W_9O_{47}$ from single-crystal X-ray diffraction data [18,24] has been preserved. This is also the case for a W-rich position that appears with high brightness (inset in Figure 3a).

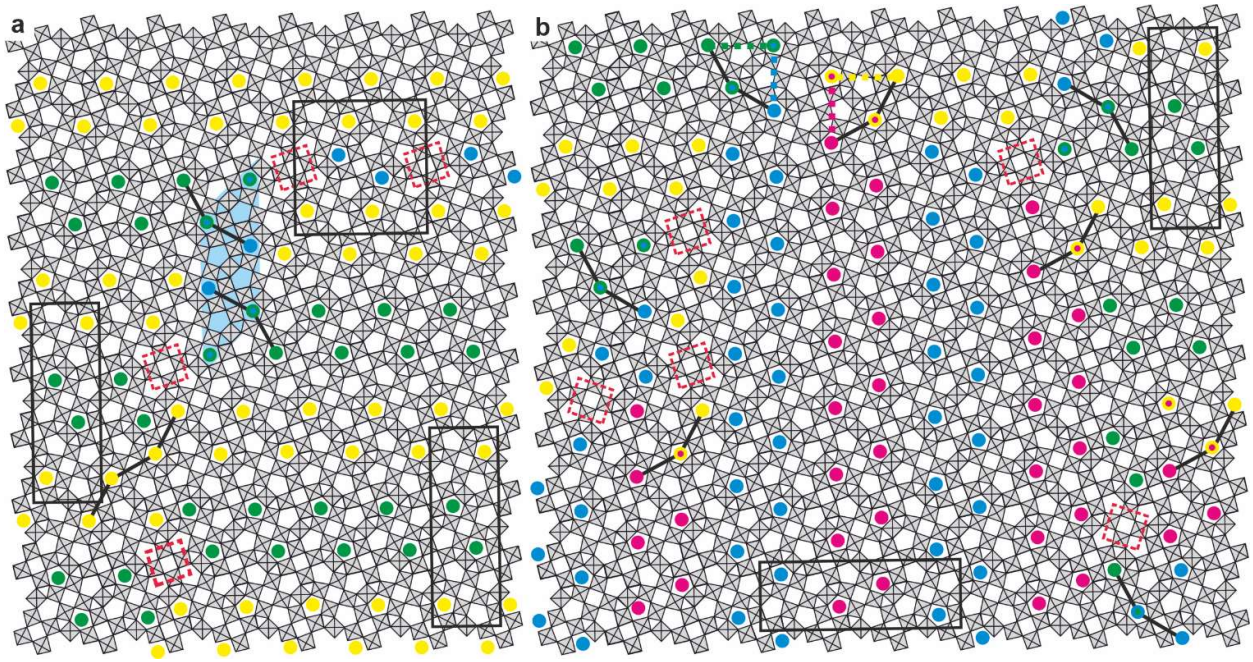

Figure 4. Structural models of the area (a) in the lower left corner and (b) in the upper right of Figure 3a. Some unit cells of $Nb_8W_9O_{47}$ and $Nb_{12}W_{11}O_{63}$ are framed black, TTB subcells with four empty PTs dotted red. In the lower part of (a), a grain boundary is present between domains of the $Nb_8W_9O_{47}$ which are shifted by 1/3 **b** with respect to each other. In (b) domains of $Nb_8W_9O_{47}$ are rotated by 90°.

The inclusion of structural units with directly adjacent PCs is a necessary means to account for the increased number of occupied PTs compelled by the decreased ratio O/ΣM. This observation is corroborated by determining the ratio O/ΣM of a rather large crystal fragment (Figure 5). As already observed in the fragments described above, this region comprises small domains with the structures of $Nb_8W_9O_{47}$ and $Nb_{12}W_{11}O_{63}$ which are intimately intergrown with each other and appear in different orientations. The occupied PTs in this large area were detected (Figure 5b) and their number was counted. The whole area contains 1345 TTB cells, in which 1876 PTs are occupied. Therefore, the overall composition is $(MO)_{1876}(M_{10}O_{30})_{1345}$ with a ratio O/ΣM = 2.755. This value is larger than that of the sample $Nb_{18}W_{16}O_{93}$ with O/ΣM = 2.735 but significantly smaller than that of $Nb_8W_9O_{47}$ with O/ΣM = 2.765.

4. Discussion

According to the evaluation of HAADF-STEM images, the sample $Nb_{18}W_{16}O_{93}$ comprises an intact TTB framework that hosts intimately intergrown domains of the $Nb_8W_9O_{47}$ phase and such with an increased amount of filled PTs. In the latter domains, the occupation of directly neighbored PTs by MO strings compensates the decreased O/ΣM: $(MO)_x(M_{10}O_{30})$ with $x > 4/3$ compared to $x = 4/3$ in $Nb_8W_9O_{47}$. This is the case in the structure of $Nb_{12}W_{11}O_{63}$ (= $(MO)_6(M_{10}O_{30})_4$ with $x = 1.5$) that has been observed in small domains in the sample $Nb_{18}W_{16}O_{93}$ for the first time. In fact, the ratio O/ΣM of $Nb_{12}W_{11}O_{63}$ (2.739) is close to that of $Nb_{18}W_{16}O_{93}$ (2.735). This dense occupation of PTs violating the first rule for a stable array of PCs is enforced by the decreased O content that must be somehow adjusted by structural adaptions. Nonetheless, the most stable PC arrangement, namely that of $Nb_8W_9O_{47}$, is still the dominating structure in the sample $Nb_{18}W_{16}O_{93}$ and present in

 doi:10.20944/preprints202111.0234.v1

many domains with typical diameters of several 10 nm. In contrast, the O-poorer domains are smaller and heavily disordered with regular structures appearing as rather small inclusions only. Both TTB superstructures $Nb_8W_9O_{47}$ and $Nb_{12}W_{11}O_{63}$ do occur in different orientation variants (Figure 5b) with the respective nanometer-sized domains coherently intergrown with each other. This flexibility is caused by the unaffected TTB-type framework with the structural modifications realized by filling PTs in different ways.

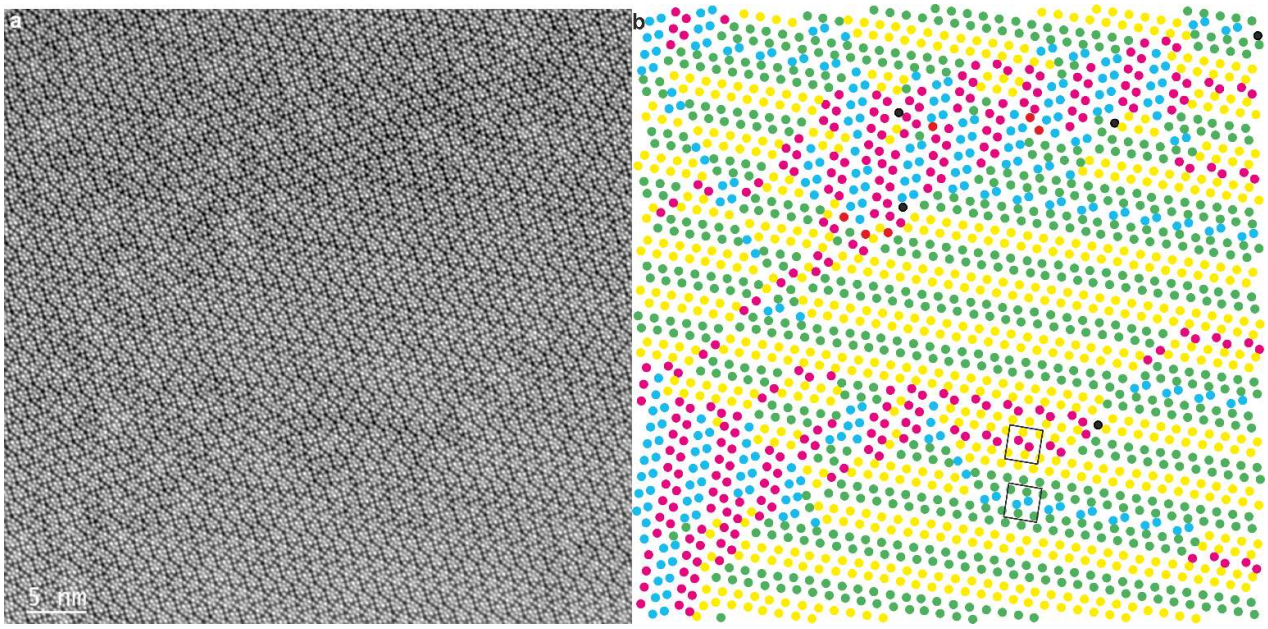

Figure 5. (a) HAADF-STEM image (courtesy of Prof. L. Shen, Nanjing) and (b) interpretation with PCs shown as filled circles. Two cells of $Nb_{12}W_{11}O_{63}$ in adjacent domains are framed.

Note that on the well-investigated W-rich side of $Nb_8W_9O_{47}$ (O/SM > 2.765 (= 47:17)), the O surplus is accommodated by forming little ordered structures with a lower density of filled PTs. An example is the $Nb_6W_8O_{39}$ structures (O/ΣM = 2.786) with four-membered PC chains (Figure 1) [4] which are intergrown with domains or even single units of $Nb_4W_7O_{31}$ (O/ΣM = 2.818) [18,25]. It is important to state that the PCs in all TTB-based structures and variants tend to be connected to form pairs or chains via the diamond link rather than being isolated or directly adjacent. In the structure $Nb_{12}W_{11}O_{63}$ corresponding to $(MO)_6(M_{10}O_{30})_4$, diamond linked PCs pairs are directly adjacent to each other which might represent a moderately stable arrangement as it is present as an intact structure in nanodomains.

5. Conclusions

The present HAADF-STEM investigation reveals that the sample $Nb_{18}W_{16}O_{93}$ cannot be considered as a separate phase. The arrangement of PCs embedded in a perfectly ordered TTB substructure corresponds in wide areas to that of the well-known and stable phase $Nb_8W_9O_{47}$ but is little ordered in small domains. No evidence for the existence of a PC array as suggested by Stephenson for the structure of $Nb_{18}W_{16}O_{93}$ [14] could be found. In general, most PCs are connected via the diamond link to form pairs or less frequently three or four membered chains of PCs. The decreased O content compared to $Nb_8W_9O_{47}$ is structurally compensated by a denser packing of PTs filled with M-O strings. This unavoidably leads to the occupation of directly adjacent PTs as they are present in the structural model proposed for $Nb_{12}W_{11}O_{63}$ here. This structure appears in the investigated sample only in nanometer-sized domains, but future synthetic efforts might be successful in indeed preparing a phase $Nb_{12}W_{11}O_{63}$ in pure form.

Funding: The APC was funded by ETH Zürich.

Acknowledgments: Sample preparation and HAADF-STEM imaging was done in the Jiangsu Key Laboratory of Electrochemical Energy Storage Technologies at Nanjing University of Aeronautics and Astronautics, People's Republic of China. I am indebted to Prof. Laifa Shen for providing the HAADF-STEM images.

Conflicts of Interest: The author declares no conflict of interest.

References

1. Griffith, K. J.; Wiaderek, K. M.; Cibin, G.; Marbella, L. E.; Grey, C. P. Niobium tungsten oxides for high-rate lithium-ion energy storage. *Nature* **2018**, *559*, 556-563. DOI: 10.1038/s41586-018-0347-0
2. Lundberg, M.; Sundberg, M.; Magnéli, A. The "pentagonal column" as a building unit in crystal and defect structures of some groups of transition metal compounds. *J. Solid State Chem.* **1982**, *44*, 32-40. DOI: 10.1016/0022-4596(82)90398-X
3. Iijima, S.; Allpress, J. G. Structural studies by high-resolution electron microscopy: tetragonal tungsten bronze-type structures in the system Nb_2O_5–WO_3. *Acta Crystallogr. A* **1974**, *30*, 22-29. DOI: 10.1107/S0567739474000039
4. Krumeich, F. Order and disorder in niobium tungsten oxides of the tetragonal tungsten bronze type. *Acta Crystallogr. B* **1998**, *54*, 240-249. DOI: 10.1107/S010876819701971X
5. Marinder, B.-O.; Hörlin, T.; Magnéli, A. Structure and ionic conductivity of $Li_x(MeO)_4Me_{30}O_{90}$ (Me = Nb^V, W^{VI}). *Mater. Res. Bull.* **1979**, *14*, 387-392. DOI: 10.1016/0025-5408(79)90104-1
6. Montemayor, S. M.; Alvarez Mendez, A.; Martínez-de la Cruz, A.; Fuentes, A. F.; Torres-Martínez, L. M. Lithium insertion in two tetragonal tungsten bronze phases, $M_8W_9O_{47}$ (M = Nb and Ta). *J. Mater. Chem.* **1998**, *8*, 2777-2781. DOI: 10.1039/A804410D
7. Martinez-de la Cruz, A.; Juarez Ramirez, I.; Torres Gonzalez, L. C. Electrochemical Li insertion in $Nb_{8-x}W_{9+x}O_{47}$ ($1 \le x \le 6$). *Mater. Res. Bull.* **2003**, *38*, 525-531. DOI: 10.1016/S0025-5408(02)01057-7
8. Ye., W.; Yu, H.; Cheng, X.; Zhu, H.; Zheng, R.; Liu, T.; Long, N.; Shui, V; Shu, J. Highly efficient lithium container based on non-Wadsley-Roth structure $Nb_{18}W_{16}O_{93}$ nanowires for electrochemical energy storage. *Electrochimica Acta* **2018**, *292*, 331-338. DOI: 10.1016/j.electacta.2018.09.169
9. Ma, X.-H.; Cheng, L.; Li, L.-L.; Cao, X.; Ye, Y.-Y.; Wei, Y.-Y.; Wu, Y.-D.; Sha, M.-L.; Zi, Z.-F.; Dai, J.-M. Influence of cut-off voltage on the lithium storage performance of $Nb_{12}W_{11}O_{63}$ anode. *Electrochimica Acta* **2020**, *332*, 135380. DOI: 10.1016/j.electacta.2019.135380
10. Lakhnot, A. S.; Gupta, T.; Singh, Y.; Hundekar, P.; Jain, R.; Han, F.; Koratkar, N. Aqueous lithium-ion batteries with niobium tungsten oxide anodes for superior volumetric and rate capability. *Energy Storage Mater.* **2020**, *27*, 506–513. DOI: 10.1016/j.ensm.2019.12.012
11. Xia, R.; Sun, C.; Wang, Y.; Cunha, D. M.; Peng, H.; Zhao, K.; Huijben, M.; ten Elshof, J. E. Enhanced lithiation dynamics in nanostructured $Nb_{18}W_{16}O_{93}$ anodes. *J. Power Sources* **2021**, *482*, 228898, DOI: 10.1016/j.jpowsour.2020.228898
12. Dong, S.; Wang, Y.; Chen, C.; Shen, L.; Zhang, X. Niobium tungsten oxide in a green water-in-salt electrolyte enables ultra-stable aqueous lithium-ion capacitors. *Nano-Micro Lett.* **2020**, *12*, 168. DOI: 10.1007/s40820-020-00508-z
13. Liu, W.; Xu, M.; Zhu, M. Design of a niobium tungsten oxide/C micro-structured electrode for fast charging lithium-ion batteries. *Inorg. Chem. Front.* **2021**, *8*, 3998–4005. DOI: 10.1039/d1qi00587a
14. Stephenson, N. C. A structural investigation of some stable phases in the region $Nb_2O_5{\cdot}WO_3$–WO_3. *Acta Crystallogr. B* **1968**, *24*, 637–653. DOI: 10.1107/S0567740868002979
15. Roth, R. S.; Waring, J. L. Phase equilibria as related to crystal structure in the system niobium pentoxide-tungsten trioxide. *J. Res. Natl Bur. Stand.* **70A** (1966) 281-303. DOI: 10.6028/jres.070A.025
16. Horiuchi, S.; Muramatsu, K.; Matsui, Y. The crystal structure of $4Nb_2O_5.9WO_3$ studied by 1 MV high-resolution electron microscopy. *Acta Crystallogr. A* **1978**, *34*, 939–946. DOI: 10.1107/S0567739478001928
17. Obayashi, H.; Anderson, J. S. Intermediate phases and pseudophases in the system WO_3-Nb_2O_5: tetragonal tungsten bronze phases. *J. Solid State Chem.* **1976**, *17*, 79-89. DOI: 10.1016/0022-4596(76)90205-X
18. Wörle, M.; Krumeich, F. On the structural complexity of tetragonal tungsten bronze-type niobium tungsten oxides. *Z. anorg. allg. Chem.* **2021**, *647*, 98-106. DOI: 10.1002/zaac.202000377
19. Kirkland, A. I.; Meyer, R. R. "Indirect" high-resolution transmission electron microscopy: aberration measurement and wavefunction reconstruction. *Microsc. Microanal.* **2004**, *10*, 401-413. DOI: 10.1017/S1431927604040437
20. Kirkland, A. I.; Saxton, W. O. Cation segregation in $Nb_{16}W_{18}O_{94}$ using high angle annular dark field scanning transmission electron microscopy and image processing. *J. Microsc.* **2002**, *206*, 1–6. DOI: 10.1017/S1431927604040437
21. Krumeich, F.; Nesper, R. Oxidation products of the niobium tungsten oxide $Nb_4W_{13}O_{47}$: A high-resolution scanning transmission electron microscopy study. *J. Solid State Chem.* **2006**, *179*,1857-1863. DOI: 10.1016/j.jssc.2006.02.020
22. Krumeich, F. Intergrowth of niobium tungsten oxides of the tetragonal tungsten bronze type. *Z. Naturforsch. B* **2020**, *75*, 913–919. DOI: 0.1515/znb-2020-0107
23. Nellist, P. D. Principles of STEM imaging. In: *Scanning transmission electron microscopy*, Pennycook., S. J.; Nellist, P. D., Eds., Springer: New York, 2011, pp. 91-116.

24. Sleight, A. W. The crystal structure of $Nb_{16}W_{18}O_{94}$, a member of a $(MeO)_xMeO_3$ family of compounds. *Acta Chem. Scand.* **1966**, *20*, 1102-1112. DOI: 10.3891/acta.chem.scand.20-1102
25. Iijima, S.; Allpress, J. G. Structural studies by high-resolution electron microscopy: coherent intergrowth of the ReO_3 and tetragonal tungsten bronze structure types in the system Nb_2O_5–WO_3. *Acta Crystallogr. A* **1974**, *30*, 29-36. DOI: 10.1107/S0567739474000040